MULTICOMPONENT METAL-ORGANIC FRAMEWORKS FOR ANALYTICAL APPLICATIONS

Máster en Nanociencia y Nanotecnología Molecular

Curso 2021/2022

Norberto Medina Rodríguez

Supervisors: Jorge Pasán García and María José Trujillo Rodríguez

Laboratorio de Materiales para Análisis Químico (MAT4LL), Departamento de Química, Universidad de La Laguna (ULL), La Laguna, Tenerife 38206, Spain

E-mail: alu0101063447@ull.edu.es

ACKNOWLEDGMENTS

Funding for this work has been obtained from the Ministerio de Ciencia e Innovación through the project PID2020-115004RB-I00.

ABSTRACT

In recent years, multicomponent metal-organic frameworks (MOFs) are being studied for a wide range of applications, exploiting the potential that comes from their enhanced complexity and functionality. One of the strategies is the ligand substitution using others with similar shape and size or using the same backbone structures with different functionalizations attached to it. Among their different properties, their adsorption behavior could change, as pore size and distribution and the analyte-MOF interactions can be different. In this work, different multicomponent MOFs based on zirconium(IV) metal clusters and three different ligands were synthesized and tested for analytical applications regarding benzophenone adsorption from an aqueous solution.

INTRODUCTION

Since the discovery of metal-organic frameworks (MOFs), a large number of porous crystalline materials formed by the combination of metal clusters and organic linkers have been reported, showing a wide diversity of framework topologies, surface areas and pore size distributions [1]. Among the different preparation methods of MOFs, solvothermal self-assembly methods have been traditionally widely used. Moreover, post-synthetic methodologies (PSMs) have been widely studied. In PSMs, precise modifications can be performed upon pristine MOFs in a solid-state manner to induce improved features while retaining crystallinity [2]. As a consequence of their wide structural variety, MOFs are being considered for a broad range of applications, such as gas storage and separation, catalysis, drug delivery, energy storage, and chemical sensing, among others [3].

Nevertheless, the heterogeneity and complexity of most reported MOFs is quite limited to the use of only one type of SBU and organic ligand. In this regard, complex MOFs built from more than one type of constituents have recently been described with the aim of achieving a higher level of structure sophistication and, thus, new properties to exploit for the aforementioned applications. These mixed-components MOFs can be constructed by using different organic ligands or metal SBUs [4]. Among mixed-component MOFs, it is important to highlight multivariate (MTV) and multicomponent MOFs. MTV-MOFs are built from ligands with identical backbone attached with different functionalities, whereas in multicomponent MOFs organic linkers or SBUs are structurally and compositionally different. As these ligands share some common properties (length, donor groups, etc.), they

can be incorporated into the structure with the same probability, making them randomly occupy their positions. It is important to mention that these terms do not include all mixed-components MOFs, but only the ones in which these different constituents have the same structural role within the structure and can, therefore, be substituted for each other. This implies that their proportions have to be free to be altered, even within a certain range. The possibility to vary the proportion of these constituents provides the potential to control structural features like pore sizes and composition, increasing the tailoring control [5].

As the complexity of these heterogeneous structures grows, characterization becomes more challenging. In general, multi-technique approaches are required in these cases using X-ray diffraction (XRD) in combination with attenuated total reflectance (ATR) infrared spectroscopy, nuclear magnetic resonance (NMR), Raman spectroscopy, and atom probe tomography. In addition, theoretical calculations have been used to elucidate specific cases of mixed-component MOFs. Because of their sophistication, complexity and/or inaccessibility in conventional laboratories, new characterization techniques and tools would be desirable for scientists to understand these complex structures [5].

In the last few decades, water contamination has become a major issue due to the large number of new compounds that are being developed and used as pharmaceutical and personal care products (PPCPs), pesticides or industrial derivatives, among others. These compounds reach water resources from multiple routes, and wastewater treatment plants (WTPs) are not equipped to remove them. New treatment processes are being studied to remove these contaminants, being MOFs one of the most promising materials due to their high sorption and catalysis properties [6]. In this regard, we are aiming to study these structures for dispersive micro-solid phase extraction procedures d-μSPE, in which a small quantity of extracting material is dispersed into a small volume of aqueous sample. Our target analyte is benzophenone (BP), a UV filter used in PPCPs [7].

In this work, two different multicomponent MOFs built from a twelve-connected zirconium SBU and two different linkers were studied: a) $Zr_6O_4(OH)_4[(ndc)_{1-x}(abdc)_x]_6(H_2O)_6$ (**abdc-x**) and b) $Zr_6O_4(OH)_4[(ndc)_{1-x}(ttmuc)_x]_6(H_2O)_6$ (**muc-x**), where x takes values from 0 to 1 in 0.1 steps. ndc, abdc, and ttmuc refer to the 2,6-naphthalenedicarboxylic acid, 4,4'-azobenzenedicarboxylic acid, and *trans,trans*-muconic acid ligands, respectively. All these MOFs were prepared and characterized by powder X-ray diffraction (PXRD), ^{1}H nuclear magnetic resonance (NMR) and nitrogen physisorption. Also, the benzophenone adsorption from aqueous solution behavior was studied.

EXPERIMENTAL METHODOLOGY

- **Reagents and materials**

Zirconium(IV) chloride (>99.5%), 2,6-naphthalenedicarboxylic acid (**ndc**) (95%), *trans,trans*-muconic acid (**ttmuc**) (98%), dimethylformamide (**DMF**) (>99.8%), acetic acid (**HAC**) (96%), and ethanol (>99%) were supplied by Sigma-Aldrich (Burlington, US) and employed in the synthesis and cleansing procedures of the MOFs. The benzophenone

standard used for the analytical studies was also purchased from Sigma-Aldrich. The ligand 4,4'-azobenzenedicarboxylic acid (**abdc**) was synthesized following the previously reported methodology [8]. A standard solution of benzophenone (**BP**) at 1230 mg L^{-1} in acetonitrile (**ACN**) was prepared for the adsorption kinetics and isotherms.

Deuterated sulfuric acid (D_2SO_4) and acetonitrile (CD_3CN) purchased from Sigma-Aldrich were used for the sample preparation for NMR.

Liquid chromatography mobile phases were prepared with ACN Liquid Chromatography - Mass Spectroscopy (LC-MS) grade, supplied by VWR, Chemicals and ultrapure Milli-Q water obtained by a water purification system A10 Millipore (Watford, UK). The mobile phases were always filtered using Durapore® polyvinylidene fluoride (PVDF) membrane filters of 0.22 µm acquired from Merck KGaA (Darmstadt, Germany).

Stainless steel autoclaves and teflon solvothermal reactors, purchased from Parr Instrument Company (Illinois, USA), were used for the synthesis of the MOFs.

15 mL Pyrex® centrifuge tubes (Staffordshire, UK), PVDF (0.2 µm) Whatman™ syringe filters, supplied by GE Healthcare (Buckinghamshire, UK), and a 2 mL Fortuna Optima® glass syringe, acquired from Sigma-Aldrich, were all employed in the µ-dSPE procedure.

- **Instrumentation**

A UF 30 model oven, supplied by Memmert (Schwabach, Germany), was used for the synthesis of the MOFs. A vortex mixer and a centrifuge model 5702 acquired from Heidolph and Eppendorf™ (Hamburg, Germany), respectively, were utilized in the µ-dSPE procedure.

The phase identification of the prepared MOFs was performed with an Empyrean diffractometer from Malvern PANalytical (Almelo, The Netherlands), operating with Bragg-Brentano geometry. Data collection was accomplished using Cu-Kα radiation (λ = 1.5418 Å) over the angular range from 5.01° to 79.99°, with a total exposure time of 10 min (approximately).

Nitrogen adsorption isotherms of the MOFs, and the resulting hybrid materials, were measured with a surface area analyzer Gemini V 2365, supplied by Micromeritics (Norcross, GA, USA), at 77 K, in the range of $0.01 \leq P/P_0 \leq 1.00$. The degas temperature was 423 K for 16 hours. The Brunauer, Emmett and Teller (BET) method was used to calculate the surface area.

^{1}H NMR spectra were collected on a Bruker Avance III spectrometer at 600 MHz.

Chromatographic analysis was performed using a UHPLC 1260 Infinity II system equipped with a G7129A autosampler from Agilent Technologies (Santa Clara, USA). The instrument was equipped with a quaternary pump and a Rheodyne 7725i injection valve with a loop of 20 µL. A UV-Vis G7115A DAD, also from Agilent Technologies, was used.

The separation was accomplished using an EC-C18 InfinityLab PoroShell column (50 mm L × 4.6 mm ID × 2.7 µm particle size) from Agilent Technologies at 25 °C, and a binary mobile

phase constituted by ACN and ultrapure Milli-Q water (with a 0.1% of acetic acid), under a constant flow rate of 0.5 $mL \cdot min^{-1}$. The elution gradient employed to achieve the optimal separation of the analytes started at 50% of ACN, holding it for 1 min. Next, it was gradually increased to 90% of ACN in 8 min and, finally, to 100% in 1 min. Full loop injection was performed. The detection wavelength was set at 254 nm.

- **Procedures**

- **Synthesis of MOFs**

The different multivariate MOFs were synthesized modifying the solvothermal method described by Bon *et al.* [9] for the DUT-52(Zr) MOF. Briefly, a mixture of zirconium(IV) chloride (1 mmol, 230 mg), ndc (1-x mmol) and abdc (x mmol) or ttmuc (x mmol), x in the range from 0 to 1 in 0.1 steps, was dissolved in 20 mL of DMF and 3 ml of acetic acid. Subsequently, the mixture was transferred to a 40 mL Teflon-lined stainless-steel autoclave and heated at 120 °C for 24 h. The resulting powder material was collected by filtration, and washed three times with 15 ml of DMF and other three times with 15 ml of ethanol.

All MOFs were activated under reduced pressure (400 mbar) at 100 °C for 24 h, before their utilization.

- **NMR sample preparation**

For the ^{1}H NMR spectra measurement, approximately 1 mg of MOF was placed in a NMR tube and dissolved in 2-3 drops of D_2SO_4 by vortex agitation. Then, the mixture was diluted to 3 mL of CD_3CN and vortex agitation and temperature were used for its dispersion.

- **Analytical procedures**

For the adsorption kinetics, 20 mg of MOF were added to a 20 mL vial, and 10 mL of a solution of an aqueous solution of benzophenone (10 mg L^{-1}) was added. The material was dispersed by orbital agitation at 225 rpm during all the procedure. At certain times, aliquots of 100 µL or 10 µL were sampled, diluted with ultrapure water up to 1 mL, and filtered through 0.2 µm PVDF syringe filters previous to their injection in the HPLC-DAD.

Similar to the adsorption kinetics, for the adsorption isotherms of the MOFs, 20 mg and alternatively 5 mg of MOF were added to 10 mL solutions of benzophenone at different concentrations. After 24 h under agitation, aliquots of 100 µL or 10 µL were sampled, diluted with ultrapure water up to 1 mL, and filtered through 0.2 µm PVDF syringe filters previous to their injection in the HPLC-DAD.

For the analytical quantification of benzophenone in the HPLC-DAD, external calibration was used. The calibration curve was prepared in the 100-1000 mg L^{-1} concentration range.

With this purpose, the standard solution of benzophenone was diluted in water to the desired concentration.

RESULTS AND DISCUSSION

- Synthesis and PXRD

The multicomponent MOF synthesis strategy has been using different ligands that have similar zigzag shape and slightly different length. The employed ndc, abdc and ttmuc ligands, shown in Fig. 1, have been reported to be able to build MOFs with the same structure and **bcu** topology using the same zirconium(IV) metal cluster [10]. The synthesis of the multicomponent MOFs was carried out as described in the experimental section. A previously reported synthesis of the DUT-52(Zr) MOF [9] was modified by replacing increasing quantities of the ndc ligand by either abdc or ttmuc until reaching a 100% ligand substitution.

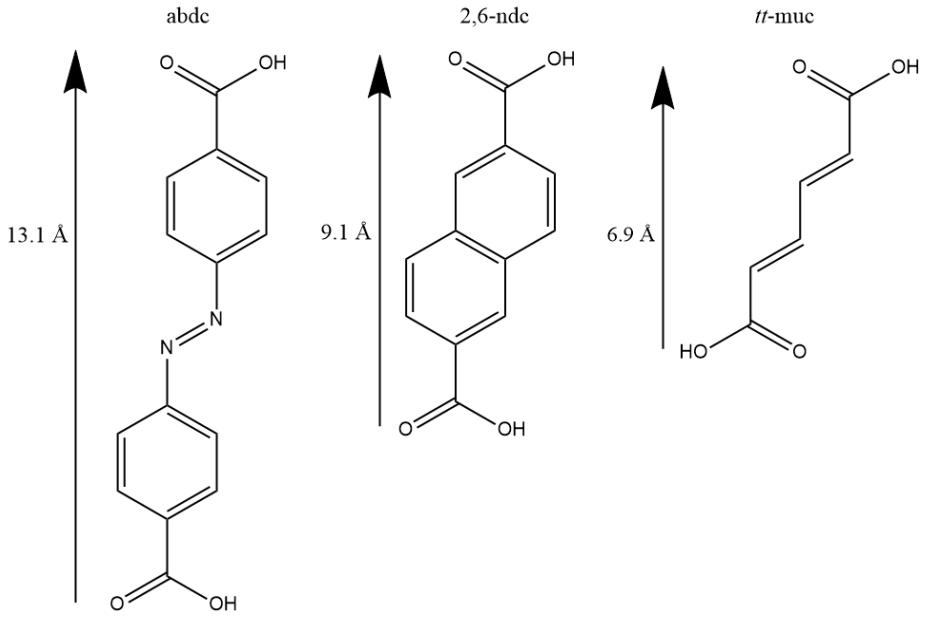

Figure 1. Comparison of the employed linkers.

PXRD patterns obtained for some of the resulting samples are shown in Fig. 2 and Fig. 3. In both cases, it is observed in the simulated patterns that the peak distribution remains equal but shifted to the left in the case of the abdc-x structures, as cell parameters are increasing due to the larger size of the ligand, or to the right in the case of the muc-x structures, as the ligand is shorter.

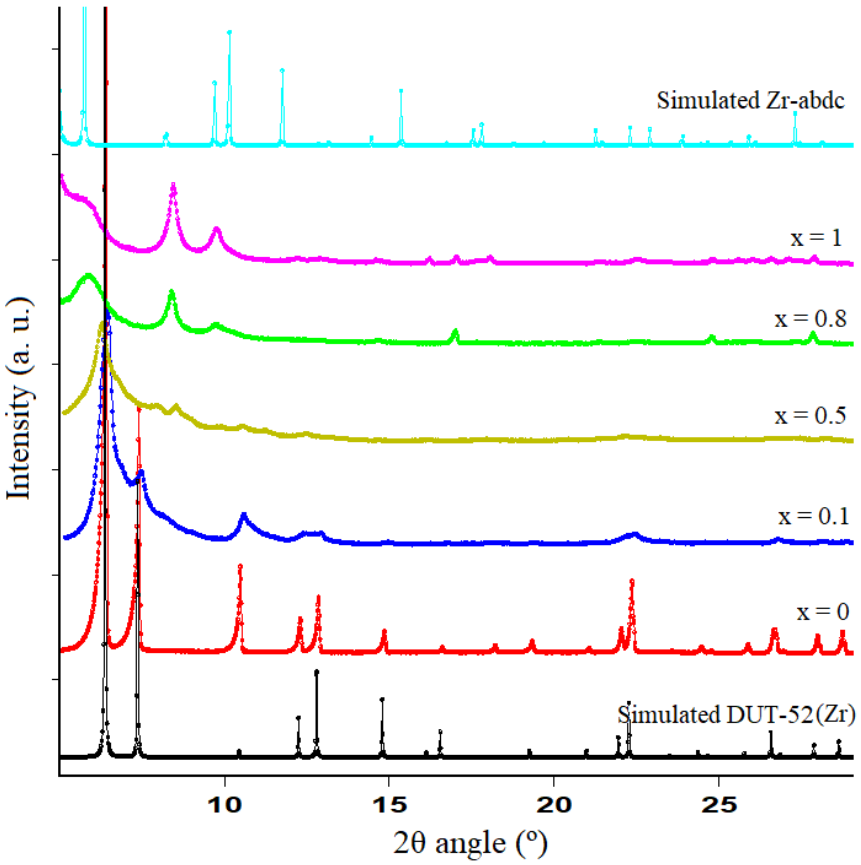

Figure 2. PXRD patterns of $Zr_6O_4(OH)_4[(ndc)_{1-x}(abdc)_x]_6(H_2O)_6$ (**abdc-x**) structures.

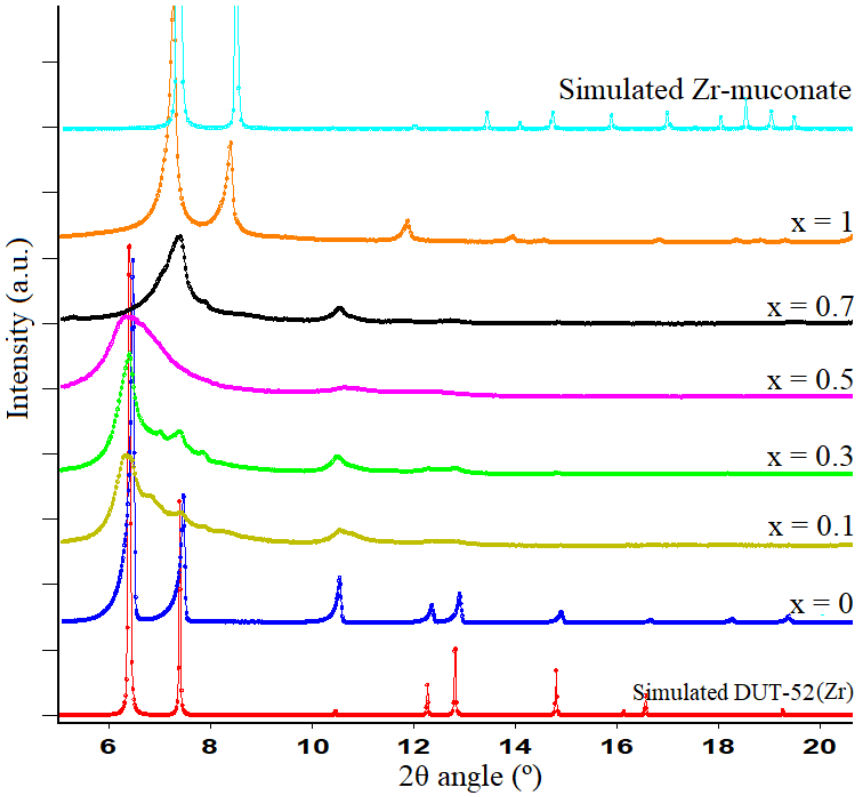

Figure 3. PXRD patterns of $Zr_6O_4(OH)_4[(ndc)_{1-x}(ttmuc)_x]_6(H_2O)_6$ (**muc-x**) structures.

In our structures we observe the same behavior, although the poor crystallinity of the intermediate structures makes it a little more difficult to notice, as the peaks are less sharp and not well defined at high angles. This poorer crystallinity is due to the lower periodicity that comes from using two different ligands with different size in the structure. Also, the employed conditions for the synthesis of all the prepared MOFs were optimized for the DUT-52 MOF, but not for the other pure structures (abdc-1 and muc-1). It has been reported that high crystalline abdc-1 structures can be achieved using high quantities of benzoic acid as modulator [11]. Therefore, a change in the synthesis conditions could make the obtained samples more crystalline.

In Fig.3 can also be noticed that for x = 0.1 and x = 0.3 there are some phase impurities that are associated with a different constituents assembly, namely a DUT-84 structure, which can be obtained as pure phase using slightly different synthetic conditions [9]. Also, for the muc-0.7 pattern it can be seen that the principal peak has shifted from around 6º to around 7.5º but the peak around 10º has not shifted yet. This could be explained by stating that the ligand incorporation is not randomly directed, but it incorporates first in some directions, affecting specific lattice planes and not others.

- **^{1}H NMR spectra**

^{1}H NMR spectra measurement is used for quantification of the linker ratio in multicomponent MOFs, and the most common sample preparation procedures are similar to that described in the methodology section [12]. As the chemical environment of some of the hydrogen atoms of the different ligands employed is different, new peaks should appear at different chemical displacements when we combine both ligands in the same sample. The relative area of those peaks would give information about their relative proportion in the sample. The spectra for abdc-x and muc-x at different ligands compositions are shown in Fig. 4 and Fig. 5. Surprisingly, the NMR spectra are quite similar for all de samples, most likely some interference coming from the decomposition of the MOF is precluding the correct analysis of the spectra.

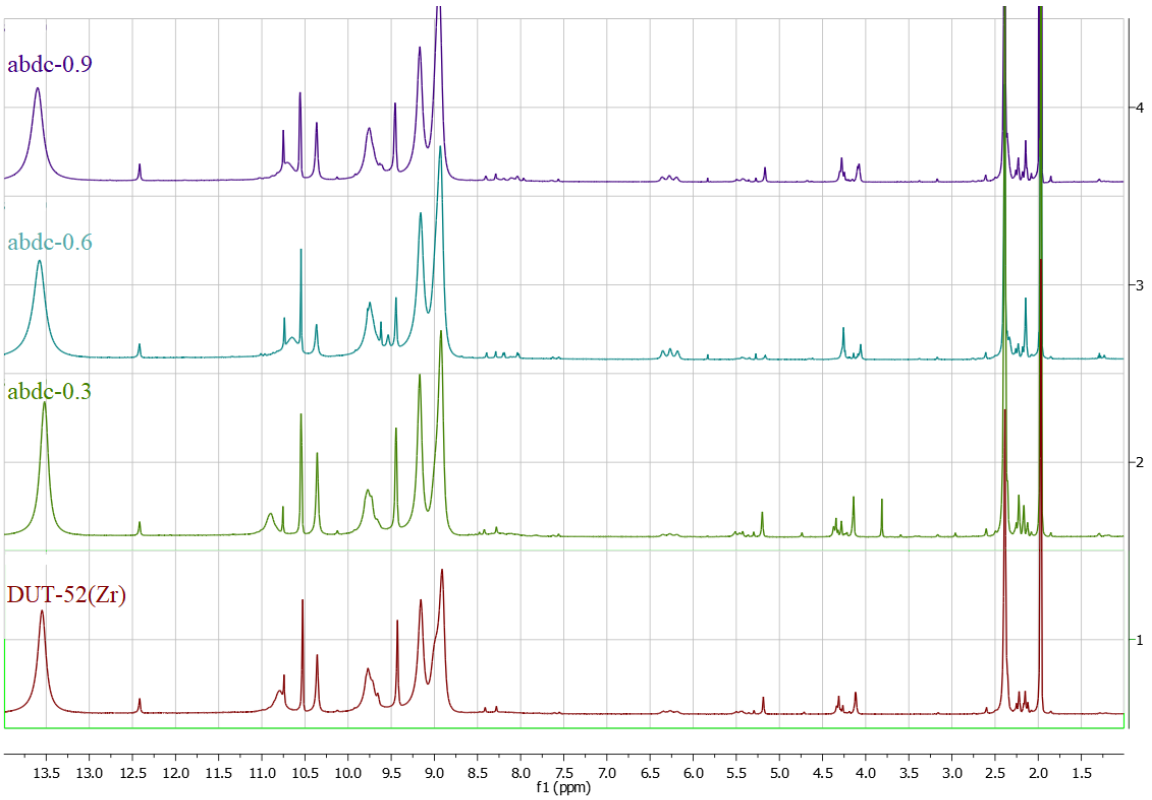

Figure 4. ^{1}H NMR spectra measurement of $Zr_6O_4(OH)_4[(ndc)_{1-x}(abdc)_x]_6(H_2O)_6$ (**abdc-x**) structures.

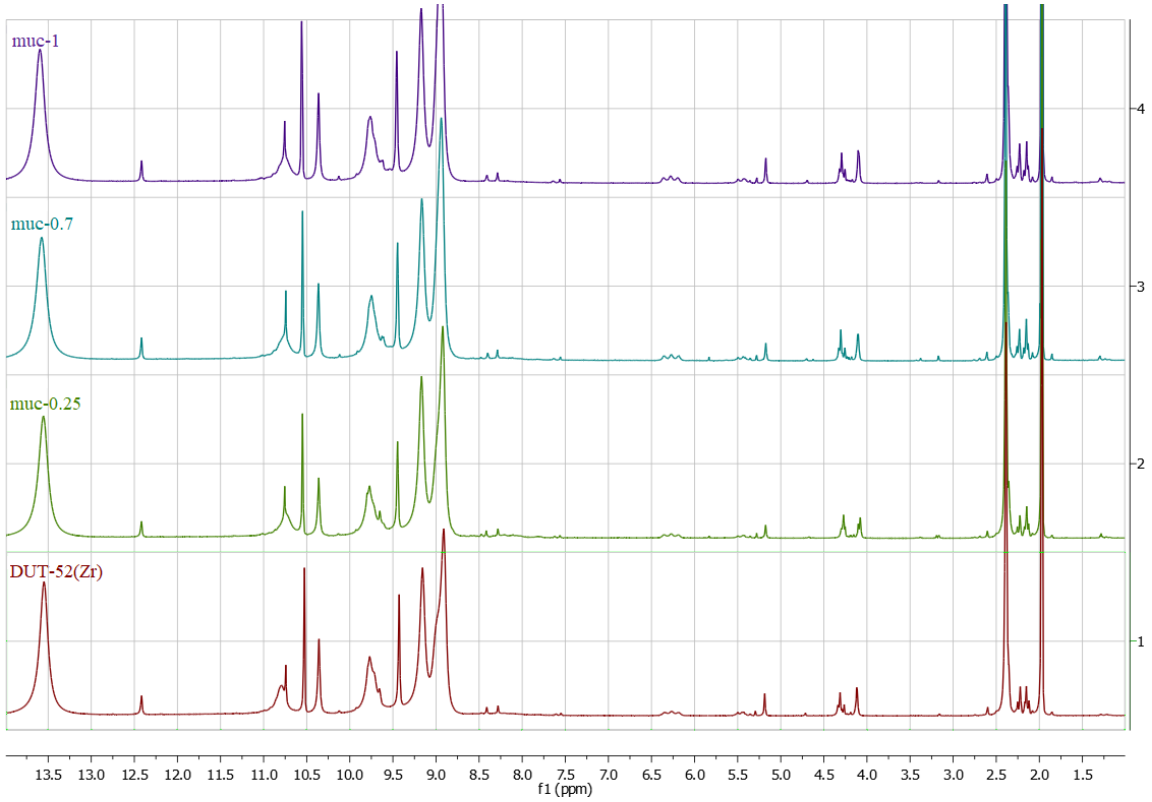

Figure 5. ^{1}H NMR spectra measurement of $Zr_6O_4(OH)_4[(ndc)_{1-x}(ttmuc)_x]_6(H_2O)_6$ (**muc-x**) structures.

- **Gas adsorption isotherms**

The obtained nitrogen adsorption isotherms can be found in the Supporting Information. According to the IUPAC isotherm classification, the isotherms of muc-0.3, muc-0.7, muc-1, and abdc-0.25 are classified as type I, while the isotherms of abdc-0.7 and abdc-1 are classified as type II. Type I isotherms are associated with microporous materials (pore diameter < 2 nm), while type II isotherms are associated with non-porous or macroporous materials (pore diameter > 50 nm) [13]. The isotherms fittings to a Brunauer-Emmett-Teller (BET) model (Eq. 1) and to a Langmuir model (Eq. 2) lead to the parameters shown in Table 1. DUT-52(Zr) data comes from previously reported measurements [9].

$$v_{\mathrm{a,BET}} = \frac{V_{\mathrm{m,N}} x}{(1-x)} \frac{C_{\mathrm{N}}}{1+(C_{\mathrm{N}}-1)x} \qquad \text{(Equation 1)}$$

$$C_{\mathrm{N}} = \exp\left(\frac{E_1 - E_{\mathrm{L}}}{RT}\right)$$

$$q_e = Q_M \frac{b\,C_e}{1+bC_e} \qquad \text{(Equation 2)}$$

where $v_{a,BET}$ (cm^3g^{-1}) is the adsorbed amount of gas, $V_{m,N}$ (cm^3g^{-1}) is the monolayer adsorption capacity, E_1 (J mol^{-1}) is the activation energy for the adsorption in the first layer, E_L (J mol^{-1}) is the activation energy for the adsorption in the second and next layers, x is the relative pressure, q_e (mg g^{-1}) is the quantity of analyte adsorbed by the material, C_e (mg L^{-1}) is the concentration at the equilibrium, Q_M (mg g^{-1}) is the maximum analyte adsorption, b (L mg^{-1}) is a constant related to the adsorption energy [14].

MOF	BET surface area (m^2 g^{-1})	Langmuir surface area (m^2 g^{-1})	Pore volume (cm^3 g^{-1})	Pore size (Å)
DUT-52	1399	-	0.60	-
muc-0.3	543	779	0.30	22.0
muc-0.7	565	809	0.31	22.0
muc-1	801	1114	0.41	20.8
abdc-0.25	855	1227	0.45	21.2
abdc-0.7	95	139	0.075	31.6
abdc-1	317	463	0.197	24.9

Table 1. Obtained parameters for nitrogen adsorption isotherms fitted to a Langmuir and a BET model.

Most obtained isotherms, especially the ones classified as type I, fit better to a Langmuir model rather than to a BET model, showing that the adsorption takes place in a monolayer instead of a multilayer. It is seen that the pure structures (DUT-52, muc-1 and abdc-1) have larger surface areas than the intermediate structures, possibly due to the lower crystallinity of the last ones. Specially relevant is the case of the abdc-x structures, in which surface areas decay nearly by a factor 10 when ligand substitution changes from 25% to 70%. This large difference could be explained by partial structure collapse. This could also be the explanation for the different isotherm classification for these two last structures (abdc-0.7 and abdc-1), changing from a microporous behavior to a non-porous behavior.

- **BP adsorption kinetics and isotherms**

Adsorption kinetics of the DUT-52(Zr) and muc-1 MOFs for benzophenone (**BP**) were measured as described in the experimental section. Fig. 6 and Fig. 7 show the resulting data for DUT-52(Zr) fitted to a pseudo-first order (PFO) Lagergren equation (Eq. 3) and to a pseudo-second order (PSO) Blonchard equation (Eq. 4), respectively. Fig. 8 and Fig. 9 show the same information, respectively, for the muc-1 MOF.

$$q_t = q_e(1 - e^{-k_1 t}) \qquad \text{(Equation 3)}$$

$$q_t = \frac{k_2\, q_e^{\,2} t}{1 + k_2 q_e t} \qquad \text{(Equation 4)}$$

where q_t (mg g^{-1}) is the amount of analyte adsorption at time t (min), q_e (mg g^{-1}) is the amount of analyte adsorption at the equilibrium, and k_1 (min^{-1}) and k_2 (g mg^{-1}min^{-1}) are the kinetic constants [15].

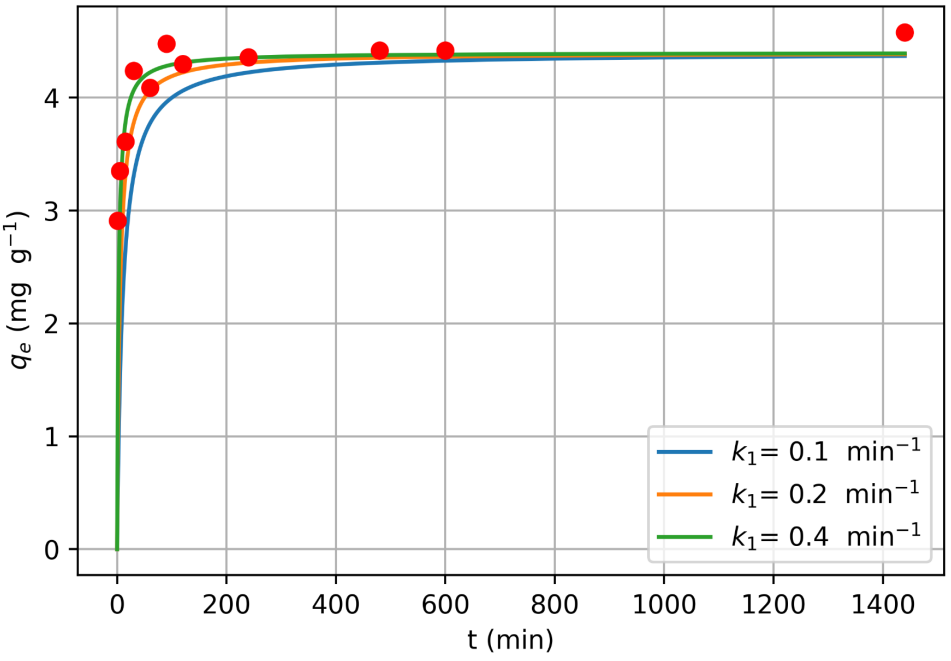

Figure 6. PFO plot for BP adsorption kinetic data of DUT-52(Zr).

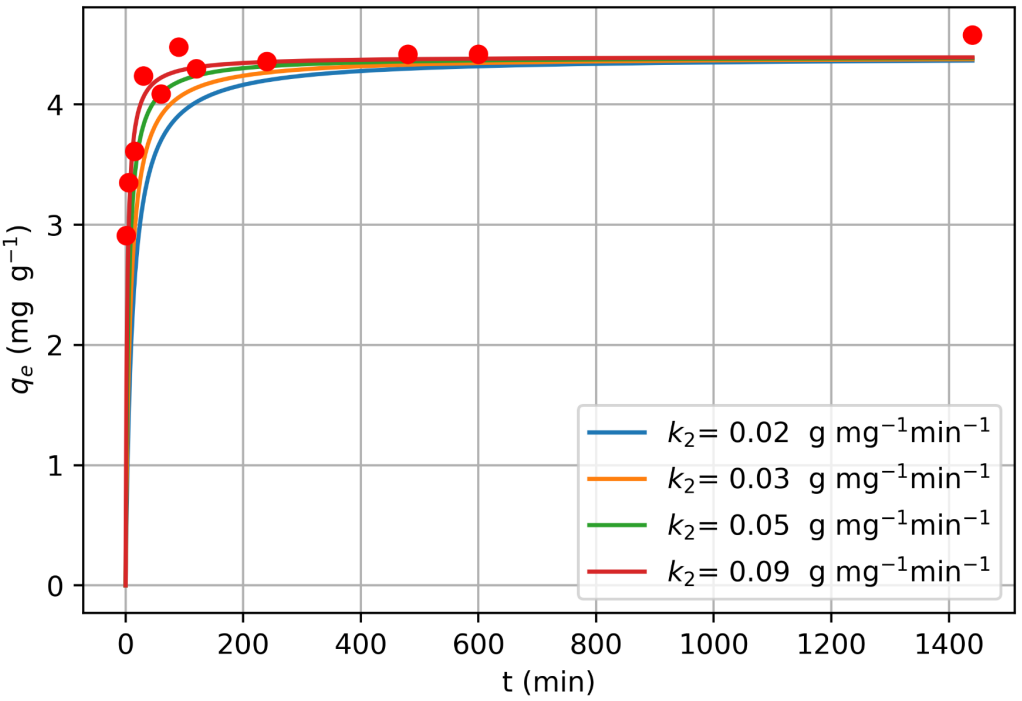

Figure 7. PSO plot for BP adsorption kinetic data of DUT-52(Zr).

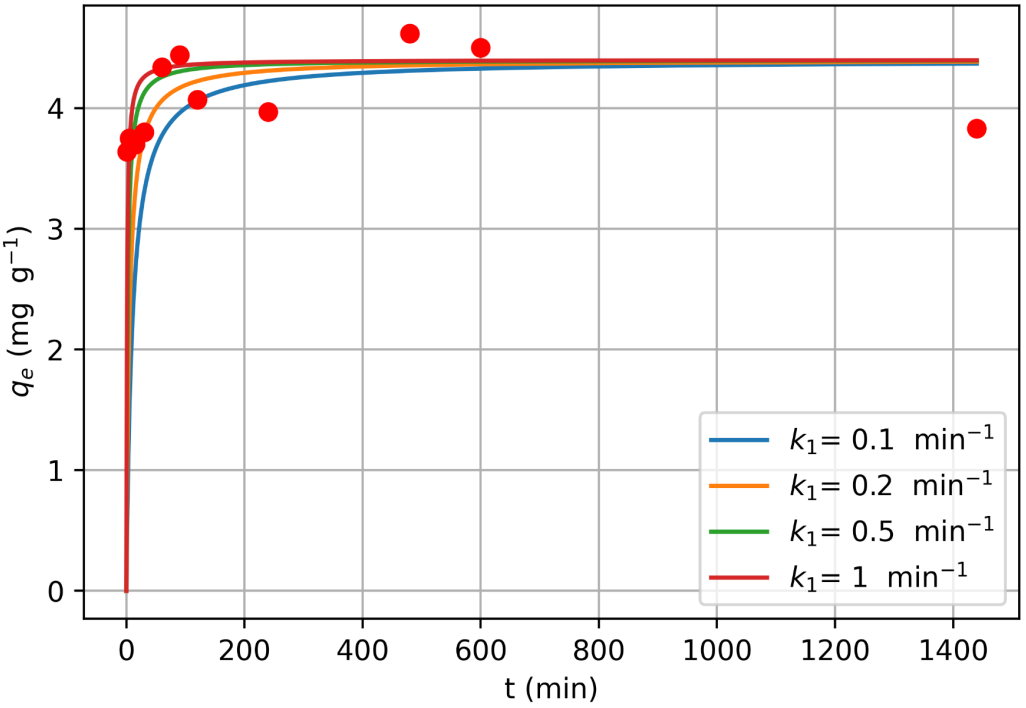

Figure 8. PFO plot for BP adsorption kinetic data of muc-1.

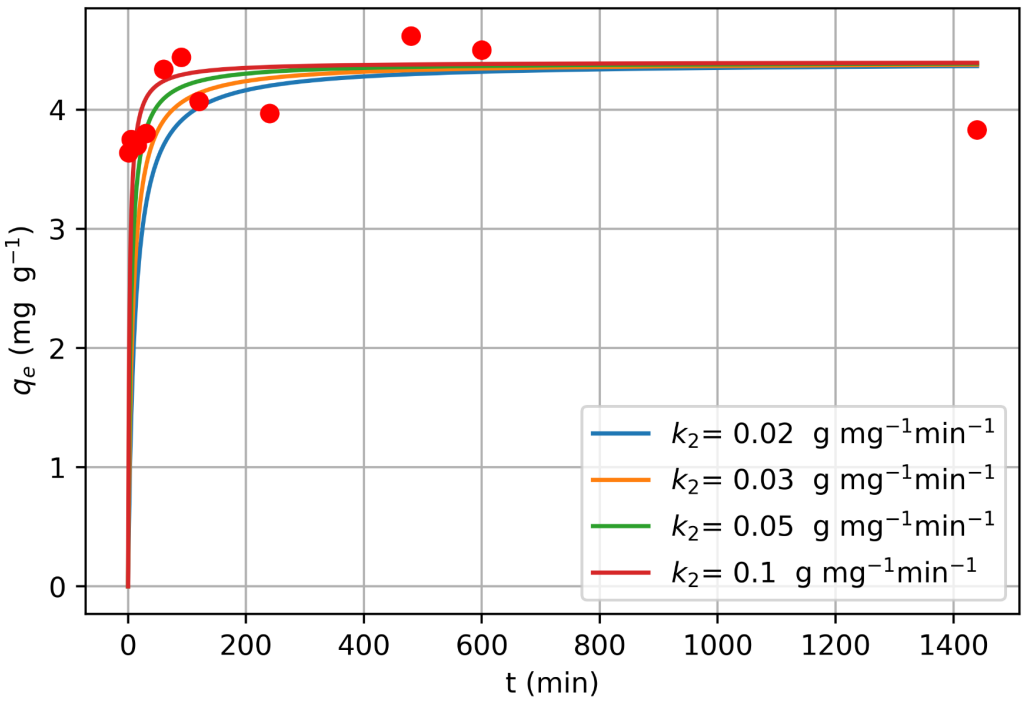

Figure 9. PSO plot for BP adsorption kinetic data of muc-1.

In both cases, the adsorption is really fast, reaching the equilibrium quickly (in less than 200 min). For this reason, non-linear fits were not studied in this case. A lower MOF quantity could be used for avoiding this situation. Some points separated from the general trend of the curves could be explained by experimental errors, which seem to have been more relevant in the muc-1 case.

Fig. 10, Fig. 11 and Fig. 12 show the resulting data for the adsorption isotherms of DUT-52(Zr), muc-1 and muc-0.7, respectively, for benzophenone, measured as described in the experimental section using 20 mg of sample. Alternatively, 5 mg of DUT-52(Zr) were also used in a second experience, shown in Fig. 13. All the data was fitted to a Langmuir adsorption model equation (Eq. 2) and to a Freundlich adsorption model equation (Eq. 5).

$$q_e = KC_e^{1/n} \qquad \text{(Equation 5)}$$

where q_e (mg g^{-1}) is the quantity of analyte adsorbed by the material, C_e (mg L^{-1}) is the concentration at the equilibrium, K (L g^{-1}) is the Freundlich constant and n is the Freundlich exponent [16].

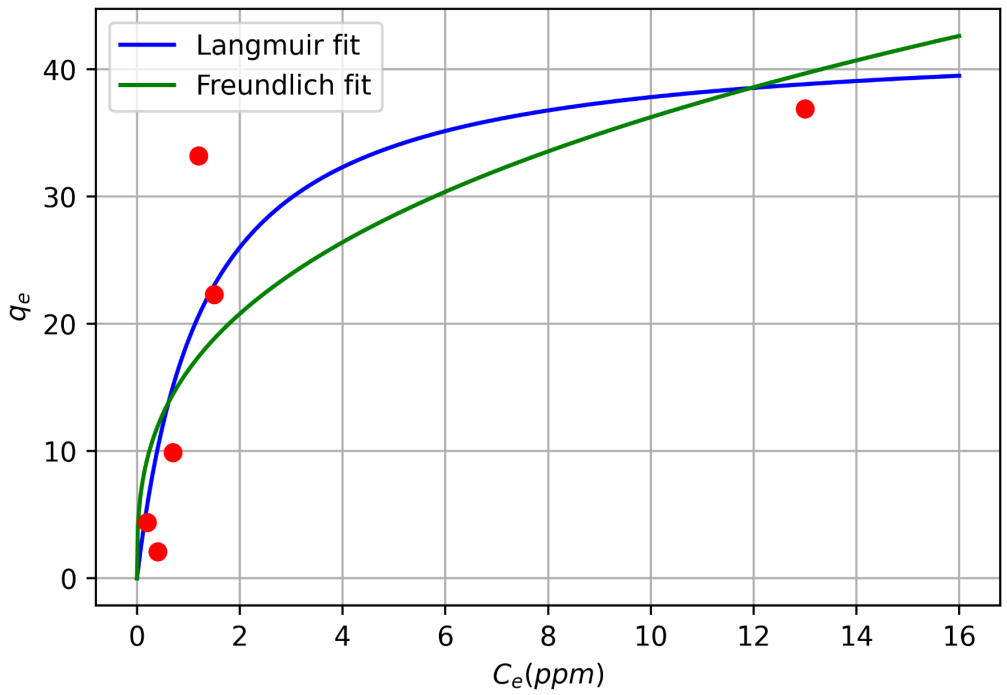

Figure 10. Adsorption isotherm data plot of DUT-52(Zr) using 20 mg. The obtained parameters are $b = 0.781$ L mg^{-1}, $Q_M = 42.7$ mg g^{-1}, $K = 16.3$ (L g^{-1}), and $n = 2.9$.

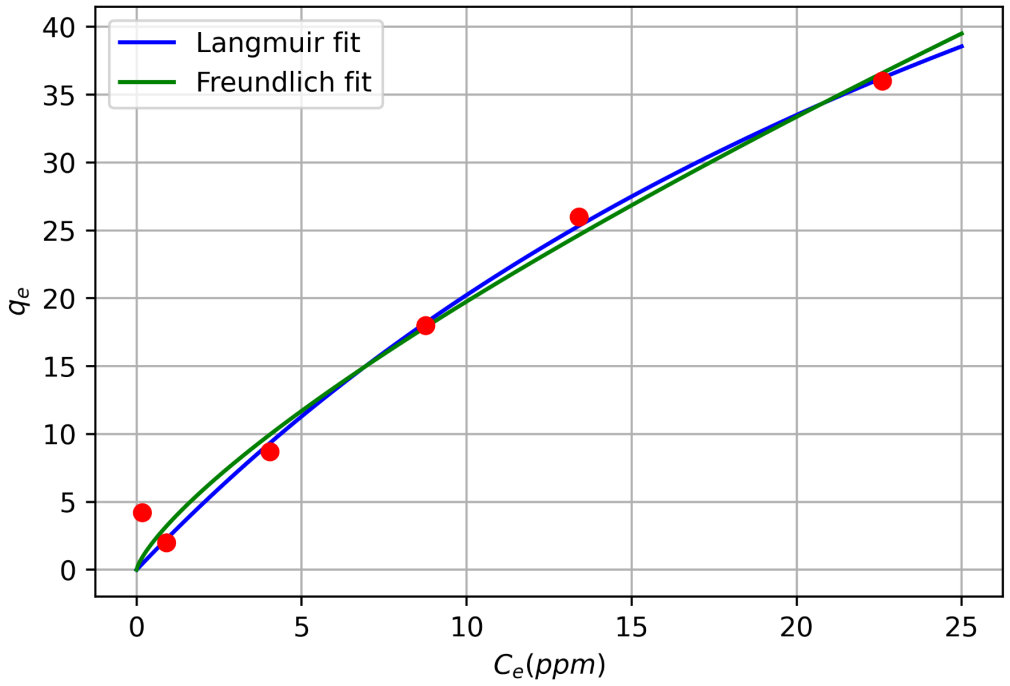

Figure 11. Adsorption isotherm data plot of muc-0.70 using 20 mg. The obtained parameters are $b = 0.0263$ L mg^{-1}, $Q_M = 97.2$ mg g^{-1}, $K = 3.47$ (L g^{-1}), and $n = 1.3$.

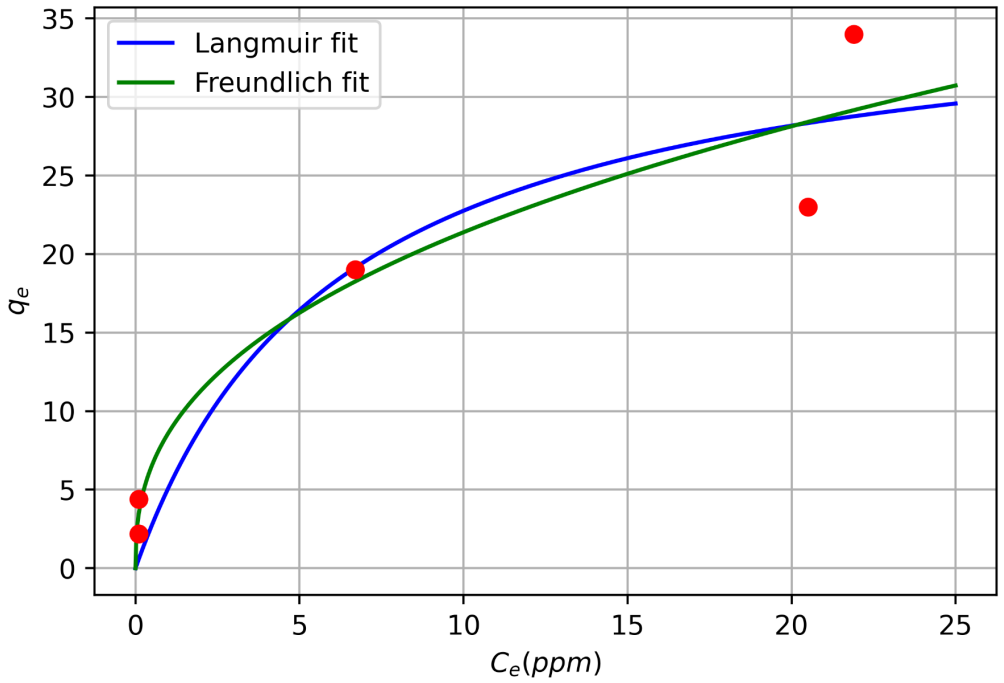

Figure 12. Adsorption isotherm data plot of muc-1 using 20 mg. The obtained parameters are $b = 0.160$ L mg^{-1}, $Q_M = 37.0$ mg g^{-1}, $K = 8.60$ (L g^{-1}), and $n = 2.5$.

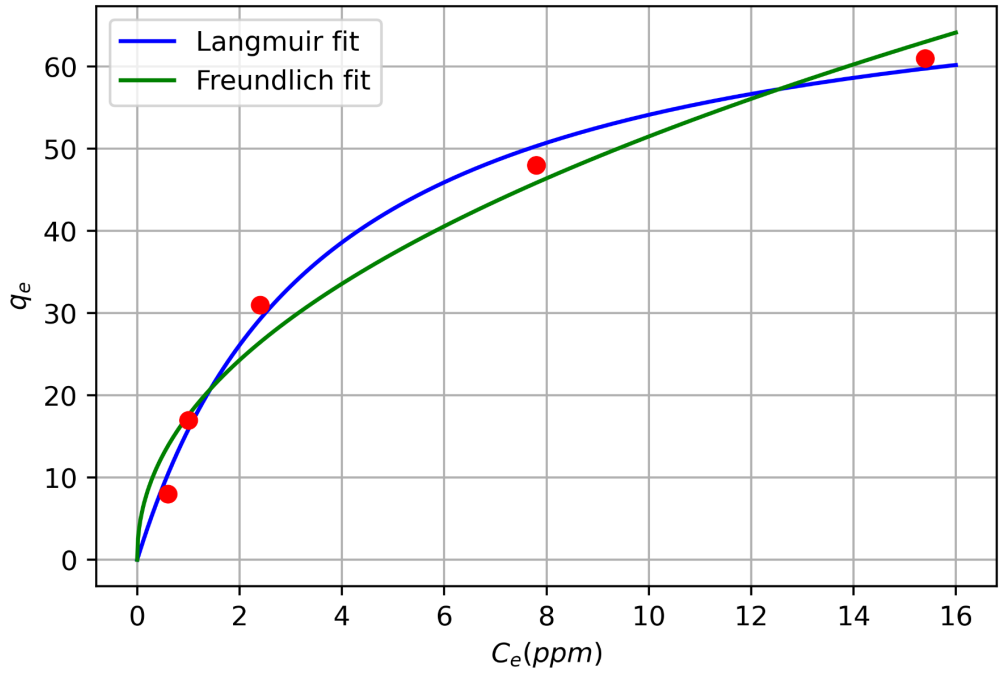

Figure 13. Adsorption isotherm data plot of DUT-52(Zr) using 5 mg. The obtained parameters are $b = 0.273$ L mg^{-1}, $Q_M = 74$ mg g^{-1}, $K = 17.6$ (L g^{-1}), and $n = 2.1$.

The data obtained in the experiences in which 20 mg of MOF were employed (Fig. 10, Fig. 11 and Fig. 12) are not representative, because the behavior of the adsorption in the studied range is approximately linear in all the studied range. For obtaining more adequate data,

lower MOF quantities should be used. In the case in which 5 mg of MOF was employed (Fig. 13), the equilibrium behavior is clearly seen.

In all the cases, the data fits better to a Langmuir model rather than to a Freundlich model. This means that the adsorption behavior occurs in a monolayer, and there is only one adsorbate molecule anchored in each adsorption site. These results are in agreement with the analyte size, that is relatively big compared with the adsorption sites in our structures. In comparison, the Freundlich model is associated with multilayer physical adsorption [17].

A calculation of the maximum BP adsorption capacity of DUT-52(Zr) (considering that 100% of possible anchoring spots adsorb one BP molecule) gives a value of 92.7 mg g^{-1}, which compared to the experimental Q_M parameter of 74 mg g^{-1} obtained leads to the conclusion that around 80% of anchoring spots of DUT-52(Zr) are able to adsorb BP molecules under these conditions for high enough BP concentrations.

CONCLUSIONS

The different multicomponent $Zr_6O_4(OH)_4[(ndc)_{1-x}(abdc)_x]_6(H_2O)_6$ and $Zr_6O_4(OH)_4[(ndc)_{1-x}(ttmuc)_x]_6(H_2O)_6$ were successfully synthesized and their phase purity was checked by PXRD. Linker ratio could not be checked using previously reported ^1H NMR procedures, so future work regarding this topic should be carried out.

Adsorption kinetics of BP show that adsorption is really quick for DUT-52 and muc-1, being this the reason why a proper linear fit could not be performed. For that, a lower MOF quantity should have been used. Finally, BP adsorption isotherms of DUT-52, muc-0.7 and muc-1 show a better adjustment to a Langmuir model rather than a Freundlich one, leading to the conclusion that there is only one anchor point for BP in the adsorption spots of the structures. Also, a high maximum capacity of 74 mg g^{-1} for DUT-52 was obtained, which would compared to the calculated maximum of 92.7 mg g^{-1} leads to the conclusion that around 80% of anchoring spots of DUT-52 are able to adsorb BP molecules under these conditions for high enough BP concentrations.

BIBLIOGRAPHY

[1] Dongwook Kim, Xinfang Liu, Myoung Soo Lah. Topology analysis of metal–organic frameworks based on metal–organic polyhedra as secondary or tertiary building units. *Inorg. Chem. Front.* **2015**, 2, 336-360.

[2] Mark Kalaj, Seth M. Cohen. Postsynthetic Modification: An Enabling Technology for the Advancement of Metal–Organic Frameworks. *ACS Cent. Sci.* **2020**, 6, 7, 1046-1057.

[3] Yuanjing Cui, Bin Li, Huajun He, Wei Zhou, Banglin Chen, Guodong Qian. Metal-Organic Frameworks as Platforms for Functional Materials. *Acc. Chem. Res.* **2016**, 49, 3, 483-493.

[4] Andrew D. Burrows. Mixed-component metal-organic frameworks (MC-MOFs): enhancing functionality through solid solution formation and surface modifications *Cryst. Eng. Comm.* **2011**, 13, 3623-3642.

[5] Marta Viciano Chumillas, Xiangyu Liu, Antonio Leyva Pérez, Donatella Armentano, Jesús Ferrando Soria, Emilio Pardo. Mixed component metal-organic frameworks: Heterogeneity and complexity at the service of application performances, *Coord. Chem. Rev.* **2022**, 451, 214273, 0010-8545.

[6] Sara Rojas, Patricia Horcajada. Metal–Organic Frameworks for the Removal of Emerging Organic Contaminants in Water. *Chem. Rev.* **2020**, 120 (16), 8378-8415.

[7] Belma Imamović, Polonca Trebše, Elma Omeragić, Ervina Bečić, Andrej Pečet, Mirza Dedić. Stability and Removal of Benzophenone-Type UV Filters from Water Matrices by Advanced Oxidation Processes. *Molecules* **2022**, 27, 1874.

[8] El-Refaie Kenawy, El-saied Aly, F. Imam Abdel-Hay, Rehab Abdeen, Yehia A.-G. Mahmoud. Synthesis and microbial degradation of azopolymers for possible applications for colon specific drug delivery I. *J. Saudi Chem. Soc.* **2011**, 15, 4, 327-335.

[9] Volodymyr Bon, Irena Senkovska, Manfred S. Weissb, Stefan Kaskela. Tailoring of network dimensionality and porosity adjustment in Zr- and Hf-based MOFs. *Cryst. Eng. Comm.* **2013**, 15, 9572-9577.

[10] Vincent Guillerm, Thais Grancha, Inhar Imaz, Judith Juanhuix, Daniel Maspoch. Zigzag Ligands for Transversal Design in Reticular Chemistry: Unveiling New Structural Opportunities for Metal–Organic Frameworks. *J. Am. Chem. Soc.* **2018**, 140, 32, 10153-10157.

[11] Andreas Schaate, Simon Dühnen, Georg Platz, Sebastian Lilienthal, Andreas M. Schneider, Peter Behrens. A Novel Zr-Based Porous Coordination Polymer Containing Azobenzenedicarboxylate as a Linker. *Eur. J. Inorg. Chem.* **2012**, 5, 790-796.

[12] Ashlee J. Howarth, Aaron W. Peters, Nicolaas A. Vermeulen, Timothy C. Wang, Joseph T. Hupp, Omar K. Farha. Best Practices for the Synthesis, Activation, and Characterization of Metal–Organic Frameworks. *Chem. Mater.* **2017**, 29, 1, 26-39.

[13] Sedat Yurdakal, Corrado Garlisi, Levent Özcan, Marianna Bellardita, Giovanni Palmisano. Chapter 4 - (Photo)catalyst Characterization Techniques: Adsorption Isotherms and BET, SEM, FTIR, UV–Vis, Photoluminescence, and Electrochemical Characterizations. Editor(s): Giuseppe Marcì, Leonardo Palmisano. Heterogeneous Photocatalysis, *Elsevier*, **2019**, Pages 87-152, ISBN 9780444640154.

[14] Milan Králik. Adsorption, chemisorption, and catalysis. *Chemical Papers* **2014**, 68, 12, 1625-1638.

[15] I. A. W. Tan, A.L. Ahmad, B. H. Hameed. Adsorption of basic dye on high-surface-area activated carbon prepared from coconut husk: Equilibrium, kinetic and thermodynamic studies. *J. Hazard. Mater.* **2008**, 154, 1-3, 337-346.

[16] G. Limousin, J.-P. Gaudet, L. Charlet, S. Szenknect, V. Barthès, M. Krimissa. Sorption isotherms: A review on physical bases, modeling and measurement. *J. Appl. Geochem.* **2007**, 22, 2, 249-275.

[17] Jianlong Wang, Xuan Guo. Adsorption isotherm models: Classification, physical meaning, application and solving method. *Chemosphere* **2020**, 258, 127279, 0045-6535.